Distribution Agreement

Hanqiao Cheng April, 10th, 2025

Anomalous Shot Noise and Non-Fermi Liquid Electron Transport in Bad Metal

β-phase Tantalum and Matel-to-Insulator Transition Material Tantalum Nitride

Nanojunctions

by

Hanqiao Cheng

Sergei Urazhdin

Adviser

Department of Physics

Sergei Urazhdin

Adviser

Erin Bonning

Committee Member

Justin Burton

Committee Member

2025

Anomalous Shot Noise and Non-Fermi Liquid Electron Transport in Bad Metal

β-phase Tantalum and Matel-to-Insulator Transition Material Tantalum Nitride

Nanojunctions

By

Hanqiao Cheng

Sergei Urazhdin

Adviser

An abstract of

a thesis submitted to the Faculty of Emory College of Arts and Sciences

of Emory University in partial fulfillment

of the requirements of the degree of

Bachelor of Science with Honors

Department of Physics

2025

Abstract

Anomalous Shot Noise and Non-Fermi Liquid Electron Transport in Bad Metal β-phase Tantalum and Matel-to-Insulator Transition Material Tantalum Nitride Nanojunctions

By Hanqiao Cheng

We measured electronic shot noise in vertical junctions of bad metal β-phase tantalum and the metal–insulator–transition material tantalum nitride (TaN). For β-phase tantalum, the length dependence of Fano factor has the same trend as the Fermi-liquid metal Ag. However, the characteristic length scale is much smaller in β-phase tantalum, suggesting an anomalous electron thermalization mechanism and a possibility of strong correlation. In TaN vertical junctions, F = 1/3 was found length ranging from 4nm to 20nm, corresponding to diffusive transport in the Fermi-liquid picture. To evaluate the disorder of TaN crystal lattice, we designed and analyzed the setup and procedure of Hall measurements on TaN Hall bars. Our investigation can provide evidence of non-Fermi liquid system and inspiration on electron thermalization mechanism in bad metals and metal-to-insulator transition materials.

Anomalous Shot Noise and Non-Fermi Liquid Electron Transport in Bad Metal β-phase Tantalum and Matel-to-Insulator Transition Material Tantalum Nitride Nanojunctions

By

Hanqiao Cheng

Sergei Urazhdin

Adviser

A thesis submitted to the Faculty of Emory College of Arts and Sciences

of Emory University in partial fulfillment

of the requirements of the degree of

Bachelor of Science with Honors

Department of Physics

2025

Acknowledgements

I want to thank Prof. Sergei Urazhdin for his invaluable mentorship, support, and guidance throughout this project. I also want to thank Mateusz Szrurek for his thorough training, technical support, and guidance. Special thanks to my friend Zilu Pang and my girlfriend Shuwen Yang, whose assistance in the lab and encouragement to me have helped me overcome challenges and stay motivated. Finally, I want to thank my group members Yiou Zhang and Sergei Ivanov for their collaboration, feedback, and the supportive working environment they helped to create.

Table of Contents

List of Figures

Chapter 1

Introduction

In 1956, Landau first introduced a theory describing the many-body quantum states of electrons in metals. This theory, later developed by Alexei Abrikosov and Isaak Khalatnikov, is well known as the Landau-Fermi liquid theory. As a generalization of the Fermi gas theory which models the quantum states of non-interacting electrons, Landau-Fermi liquid theory takes into account electrons' interaction with themselves and surrounding particles such as phonons[1]. The excited states of interacting electrons are characterized as quasi-particles. However, in many anomalous quantum materials, such as high-temperature superconductors[2], Mott insulators[3], and strange metals[4], the quasi-particle pictures of energy excitations of electrons can breakdown. The investigation of non-Fermi liquid systems has provided valuable insights into condensed matter physics[5].

"Bad metals" are considered as strong candidates of non-Fermi liquid systems. In a normal metal, the electron mean free path l is much larger than the lattice spacing a, resulting in conventional metallic behaviors including small resistivity, positive temperature coefficient of resistivity(TCR), and saturation of resistance over high temperature[6]. However, in materials known as "bad metals", disorder or defects of the crystal lattice cause the electrons to scatter so frequently that l can be comparable to a. In this case, electrons scatter so often that they hardly have space to form quasi-particles. This results in the very high resistivity $\rho > 1.5\mu\Omega$m in bad metals, approaching the Ioffe-Regel limit[7]. At the high temperature limit, bad metals exhibit a non-saturating dependence of resistivity on temperature, which suggests a breakdown of Fermi liquid picture of electron transport and a strong correlation of electrons[8].

How can we probe the transport properties and correlation states of electrons in bad metals? Shot noise—the fluctuation of current in metallic conductors due to the discrete nature of electrons—was proved as a powerful tool[9]. Here we briefly review the theoretical framework of shot noise. Theoretically[10], at zero temperature limit when electron transport can be described by a Poissonian process–randomly with no interaction with each other or other particles–the expression of shot noise is

$$S_{IPoissonian} = 2e\langle I \rangle, \tag{1.1}$$

where $S_{IPoissonian}$ is the power spectral density of the Poissonian noise, e is the elementary charge, and $\langle I \rangle$ is the average current bias. The Fano factor of shot noise is defined as the ratio of the measured noise to the Poissonian noise:

$$F = \frac{S_I}{2e\langle I \rangle}. \tag{1.2}$$

At finite temperature, the thermal agitation of charge carriers generate Johnson-Nyquist noise:

$$S_J = \frac{4k_B T}{R}, \tag{1.3}$$

where S_J is the current noise spectral density, k_B is the Boltzmann constant, T is the temperature, and R the resistance of the conductor. Considering Johnson noise and electron thermalization, the voltage-based expression for shot noise is

$$S_V = 4k_BT_eR + 2e\langle V\rangle RF\left[\coth\left(\frac{eV}{2k_BT_e}\right) - \frac{2k_BT_e}{eV}\right]. \tag{1.4}$$

We define $V_{th} = \frac{2k_BT}{Fe}$ as the crossover voltage from the Johnson-noise-dominated regime to the shot-noise dominated regime[11][12]. With this definition, equation (1.4) can be written as

$$S_V = 2FeR\left(V\coth\frac{V}{V_{th}} - V_{th}\right) + 4k_BTR. \tag{1.5}$$

The thermal broadening factor is defined as $B = \frac{eV_{th}}{2k_BT}$. The details of these definitions will be further discussed in Chapter 3. The values of F and V_{th} for a given sample are obtained by fitting the S_V vs. V data to Equation (1.5) and letting F and V_{th} be fitting parameters.

The Fano factor F and thermal broadening factor B can provide crucial information about the dominant scattering mechanism of electrons in a conductor[4][13][14]. The scattering mechanism is characterized by the scattering mean free paths. Under the Fermi-liquid picture, when the length of the conductor L satisfies l_{e-e}, $l < L < l_{e-e}$, where l is the electron-impurity scattering mean free path and l_{e-e} is the electron-electron inelastic scattering mean free path, $F = \frac{1}{3}$[13] and $B = 1$[15]. In this regime, electron transport is diffusive. When $l_{e-e} < L < l_{e-ph}$, where l_{e-ph} is the electron-phonon scattering mean free path, $F = \frac{\sqrt{3}}{4}$ and $B = \frac{2}{\sqrt{3}}$[16]. In this "hot electron regime", electrons are thermalized due to strong inelastic scattering. Using the Boltzmann-Langevin formalism, a recent theoretical study has shown that $F = \frac{\sqrt{3}}{4}$ indicates a strong correlation of electrons in a diffusive Fermi-liquid system[9]. Finally, when $L > l_{e-ph}$, electron-phonon scattering dominates, shot noise is suppressed as $1/L^{\alpha}$, where α depends on the material. A summary of the length dependence of Fano factor a Fermi-liquid metal Ag at temperature 50mK is shown in Figure 1.1.

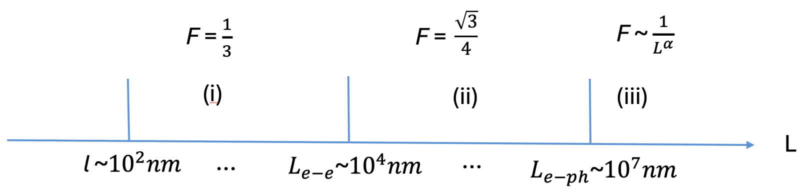

Figure 1.1: Electron scattering mean free paths and corresponding shot noise Fano factor of a Fermi-liquid metal Ag at temperature 50mK.

A deviation of the Fano factor of shot noise from these characteristic values suggests a breakdown of the Fermi-liquid picture. In a recent shot noise study on nanowires of a heavy fermion strange metal $YbRh_2Si_2$, the Fano factor of shot noise was found strongly suppressed under the Fermi-liquid values–around 0.1 at base temperature 3K–and decreased with increasing temperature[4]. This is not predicted by the shot noise theory based on Fermi-liquid theory[13]. Ruling out the effect of electron-phonon scattering as a dominant scattering mechanism, the authors attributed the suppression of shot noise in $YbRh_2Si_2$ to the strong correlation of electron and breakdown of the quasi-particle pictures.

As a transition metal with very high corrosion resistance, melting point, and stability, tantalum(Ta) has been widely used for electronic capacitors, superalloys, corrosion-proof layers, and thermionic emitters in both industry and scientific research. Besides these wide applications, Ta has been shown to have interesting metallic behaviors that can contribute insights to condensed matter physics. Tantalum can form two crystal phases: body-centric-cubic α phase and metastable tetragonal β phase. Disorder, an intrinsic deviation from well-arranged or periodic crystal lattice of materials, was shown in β phase tantalum (βTa)[17] to cause weak localization of electrons and reconstruction of electron band structure[18], making a deep investigation on the potential correlated states of electron in βTa necessary.

This necessity was reassured by the anomalous resistivity(ρ) vs. temperature(T) characteristics of βTa. In our previous study[12], we measured resistivity ρ of bulk αTa and βTa samples over a temperature range from 4.3K to 300K. ρ of α phase tantalum(αTa) increases linearly as temperature. Along with the small range of $\rho < 0.3\mu\Omega$m, it is reasonable to conclude αTa as a normal metal. On the other hand, βTa exhibits a negative temperature coefficient of resistivity(TCR) and a high ρ close to 1.5$\mu\Omega$m, the Ioffe-regel limit of resistivity. The ρ vs. T characteristics of αTa and βTa are summarized in Figure 1.2. Details of the fabrication difference of these two phases of tantalum will be discussed in Chapter 3.

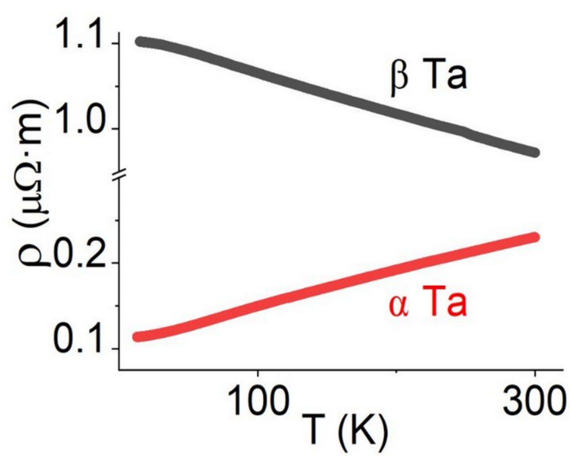

Figure 1.2: ρ vs. T for 15nm-thick βTa and αTa extended thin films through four-probe van der Paul measurement.

The bad metal behavior of βTa has motivated us to investigate its correlated states of electrons and the mechanism of electron transport through measuring shot noise of βTa nanowires with lengths ranging from 100nm to 2000nm[12]. A strong suppression of shot noise was found. For 100nm β Ta nanowires, we measured $F = 0.158 \pm 0.02$ at base temperature 4.3K, decreasing as temperature increases. We ruled out single-electron hopping transport as a dominant transport mechanism and therefore as a source of shot-noise suppression. We also modeled electron–phonon scattering with a drift–diffusion equation, but the calculated curves failed to give a reasonable fit. This simplified model of electron-phonon scattering implied that such scattering pattern cannot be dominant in βTa nanowires. The source of the suppression of shot noise in βTa nanowires was left unknown. The magnitude and temperature dependence of the Fano factor, however, were very similar to the strange metal $YbRh_2Si_2$, suggesting a strong electron–electron correlation and a breakdown of Fermi-liquid transport system in βTa. On the other hand, the length dependence of the Fano factor in βTa was also interesting. As the length of the nanowires increased from 100nm to 2000nm, F at the base temperature tended to decrease. This trend made us curious about the value that F will reach as the length continues to decrease. For example, in diffusive transport regime, $F = 2/3$ indicates a Cooper pair. With a hypothesis of the existence of the correlation of electrons in βTa, it is also worth observing the length dependence of Fano factor in βTa and comparing with the Fermi-liquid characteristics as shown in Figure 1.1. These unsolved questions have motivated us to investigate shot noise in βTa vertical junctions with L =20nm, 8nm, and 4nm.

Another part of this thesis is reporting the shot noise measurement of tantalum nitride(TaN) vertical junctions. As an important compound of tantalum, TaN has been widely studied for its interesting metallic and nonmetallic properties. It was shown to be superconducting with a phase transition temperature (T_c) ranging from 0.5 to 10.8K depending on the fabrication process, which includes nitrogen pressure during deposition and sample geometry[19].

Besides superconductivity, a recent study on TaN thin films reported a superconductor to weak-insulator transition(SIT) with a transition temperature around 10K[20]. Disorder of lattice of TaN was probed through X ray diffraction and was shown to depend on partial nitrogen pressure and the film thickness. The critical temperature of SIT in TaN was shown to depend on the nitrogen pressure.

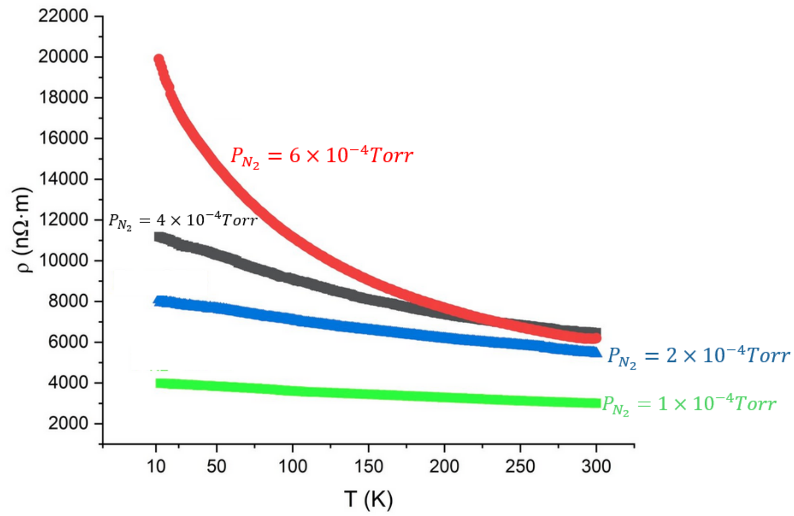

Figure 1.3: ρ vs. T characteristics of TaN extended thin films. The pressure denotes the partial nitrogen pressure added to the sputtering chamber during the sputtering process.

Interestingly, our ρ vs. T measurement on bulk TaN films varying N2 pressure showed that at a high N2 pressure, TaN exhibits a transition from a bad metal(negative TCR) to an insulator(diverging ρ at low temperature limit). A metal to insulator transition can be caused by electron localization, which can be caused by strong disorder in crystal lattice[21]. The many-electron states in such a disorder system can provide insights into the non-Fermi liquid picuture of electron transport[22]. These anomalous properties of TaN motivated us to study the electron transport properties through shot noise in TaN vertical junctions varying N2 pressure and comparing with the results of βTa vertical junctions.

Chapter 2

Methods

We first discuss the fabrication procedure of βTa and TaN vertical junctions and TaN hall bar. All sample patterns were defined by electron beam lithograph(EBL) on methyl methacrylate(MMA) and polymethyl methacrylate(PMMA) bilayer resist. Figure.2.1 shows a top view of scanning electron microscopy (SEM) image of a TaN vertical junction sample. The exposed electron beam resists were developed in an

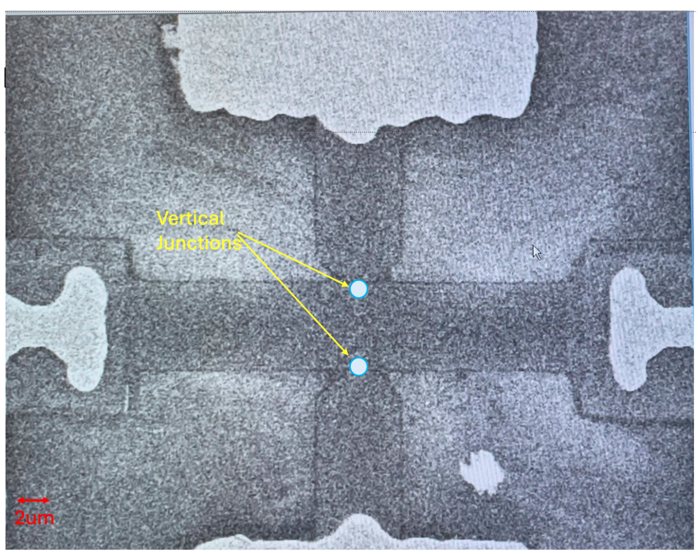

Figure 2.1: Top view SEM image of the nanopillar sample. The dark cross-shape structures are metallic electrodes that connect to the measurement circuit. The two blue dots are the effective parts of the sample–vertical junctions.

methyl isobutyl ketone (MIBK) and isopropyl alcohol (IPA) 1:2 solution for 25 seconds.

All metallic components were sputtered through magnetron sputtering deposition system and all oxides through radio-frequency(RF) sputtering deposition system. All sputtering procedures were performed in a vacuum chamber with a base pressure of 5×10^{-9} Torr with 3.8×10^{-3} Torr of ultrahigh-purity Ar. All sample structures were deposited on sapphire substrates.

We now focus on the sputtering deposition recipe of βTa and TaN vertical junctions. For βTa, the recipe of the bottom electrode was $Im(5)/Ti(2)/Cu(40)/Ti(2)/Ta(x)$, where chemical elements separated by slash from left to right represent the sequence of sputtering deposition, the number in parenthesis is the thickness in nanometers, and Im indicates Ar ion milling. For $Ta(x)$, the DC current used to ionize the Ar plasma was 0.54mA and the sputtering rate of Ta was maintained close to $0.3\mathring{A}/s$. Nitrogen gas with a partial pressure 4×10^{-6} Torr was added when $Ta(x)$ was sputtered to make sure that $Ta(x)$ sputtered on $Ti(2)$ seeding layer is in β phase, not α phase. An $Al(35)$ pillar with radius = 20nm was deposited through thermal evaporation. When the current flow through the top electrode to the effective $Ta(x)$ layer, the shunting effect confines the current to only flow through the cross-sectional area of the vertical junction. $SiO_2(13.5)$ was deposited through RF sputtering on top of $Im(30)$. On

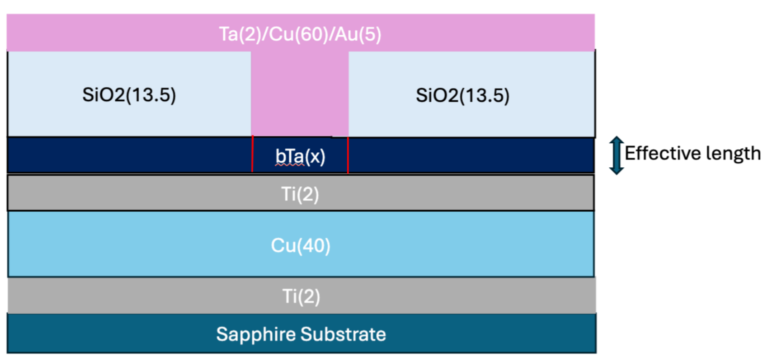

Figure 2.2: Side view design pattern of a βTa vertical junction. The red lines represent the area the current was confined by the shunting effect.

top of $SiO_2(13.5)$, Ar ion milling was performed with a tilted angle = 93°and 265°for

2min respectively. $Al(13.5)$ was etched off through rinsing in 5% NaOH solution for 90 seconds. Polymer residue was lifted off through ultrasound cleaning in acetone and was cleaned through rinsing in IPA solution. The top electrode $Ta(2)/Cu(60)/Au(5)$ was finally sputtered, where $Au(5)$ was to protect the sample from oxidation. Figure 2.2 shows the design pattern of a βTa vertical junction.

The TaN vertical junction has the same design pattern and fabrication recipe as βTa except the bottom electrode was changed to $Im(5)/Pt(1.5)/Cu(40)/Pt(1.5)/TaN(x)$, which is shown in Figure 2.3. For shot noise measurement and hall measurement, we fabricated multiple TaN samples with two different nitrogen pressure: 1×10^{-4} Torr and 4×10^{-4} Torr.

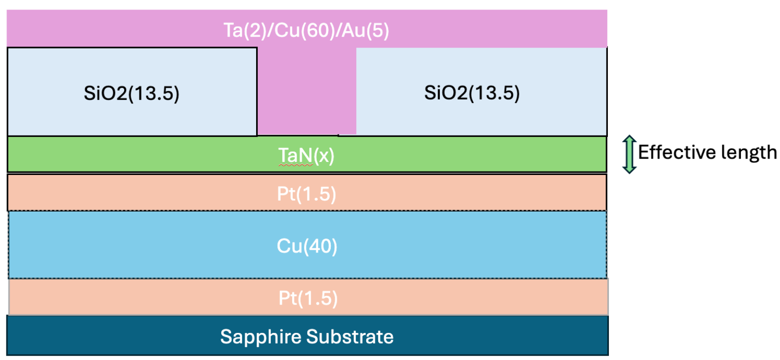

Figure 2.3: Side view design pattern of a TaN vertical junction.

The noise measurement of βTa and TaN vertical junctions was conducted in a microwave cryostat with a base temperature 4.3K. Fig.2.4 shows the circuit diagram of the measurement circuit. As mentioned, the microwave line resistance was 50Ω. The lead resistance varied among samples but were much smaller than the effective sample resistance. The temperature dependence of resistance was neglected in our experiment. The generation of shot noise requires a DC voltage bias. The bias-tee inputs a DC signal to the cryostat while separating this DC signal with the AC noise signal output by the cryostat. The noise signal was then amplified by an ultralow noise amplifier, rectified by a microwave diode, and converted to digital signal by an A/D converter. Figure 2.4 shows the circuit diagram for the noise measurement. For each sample, the Johnson noise produced by the sample was also measured over temperature range from 4.3K to 300K for unit conversion. The noise power at zero voltage bias was plotted as a function of temperature(at 4.3K, 6K, 8K, 10K, 15K, 20K, and 25K). The plot is linear since at zero voltage bias, the shot noise vanishes, and the noise we measure is only Johnson noise plus white noise(offset) which depends linearly to temperature. The slope and offset of the linear dependence was extracted for the unit conversion from the LabView results to the actual values.

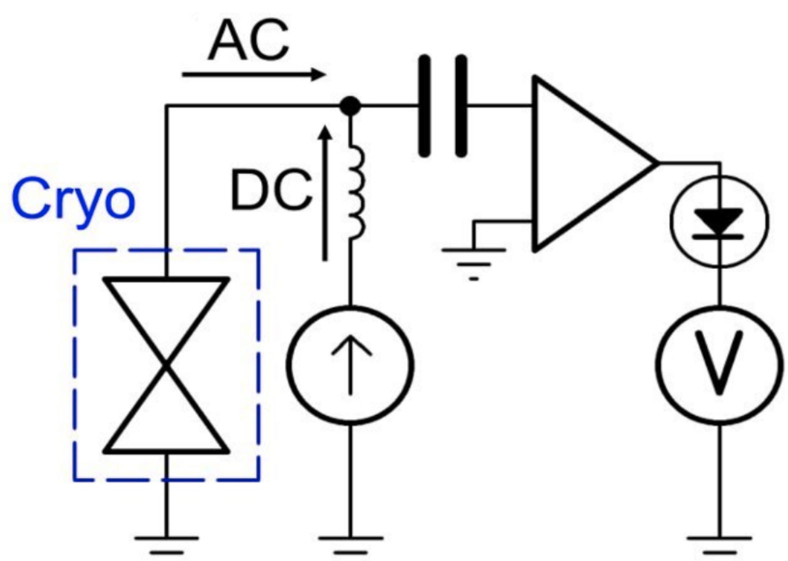

Figure 2.4: Circuit diagram for shot noise measurement set up. The AC noise signal coming from the cryostat can only pass through the capacitor path, while the DC supply can only pass through the inductor path to enter the cryostat.

We used a Greek cross design of Hall bar to measure the Hall effect of TaN. The recipe is as follows. The Hall bar $Im(5)/Pt(2)/TaN(20)/Au(5)$ was first sputtered on the sapphire substrate. $Im(7)$ was then performed to remove the $Au(5)$ layer. The four electrodes $Ta(3)/Cu(60)/Au(5)$ were finally sputtered. Figure 2.5 shows Hall measurement setup.

A Magnetic field B was applied perpendicular to the hall bar. A DC current I was applied through the horizontal and the Hall voltage V_H was measured through the electrodes in vertical direction. Figure 2.6 shows the circuit diagram for Hall measurement.

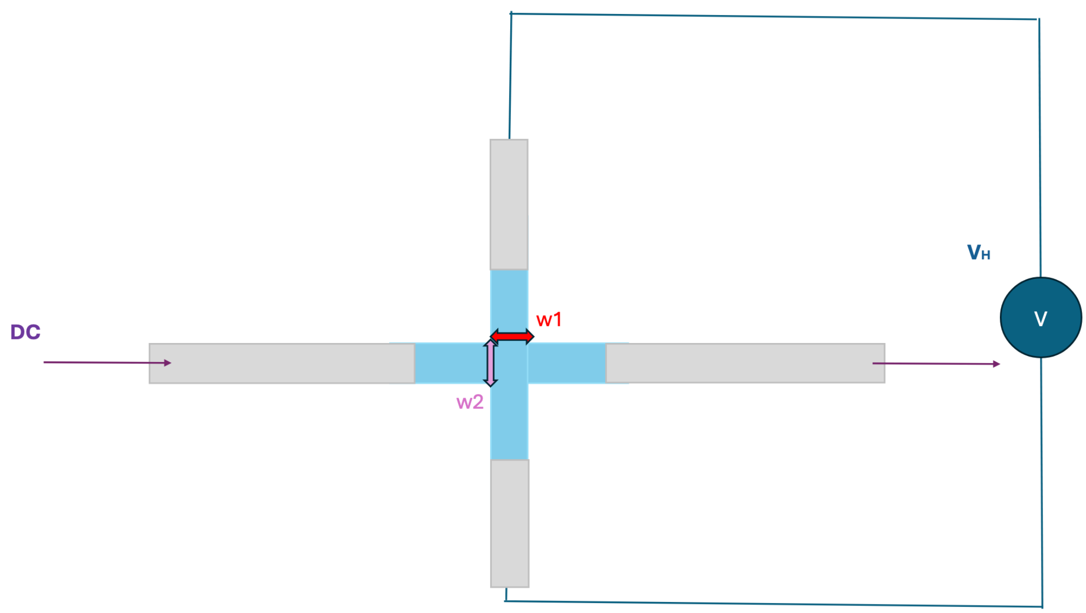

Figure 2.5: Schematic of the Hall measurement setup. The blue part is the Hall cross. The effective lengths $w_1 = 3\mu$m and $w_2 = 3\mu$m.

Chapter 3

Results and Discussion

We first discuss the shot noise measurement results of βTa vertical junctions.

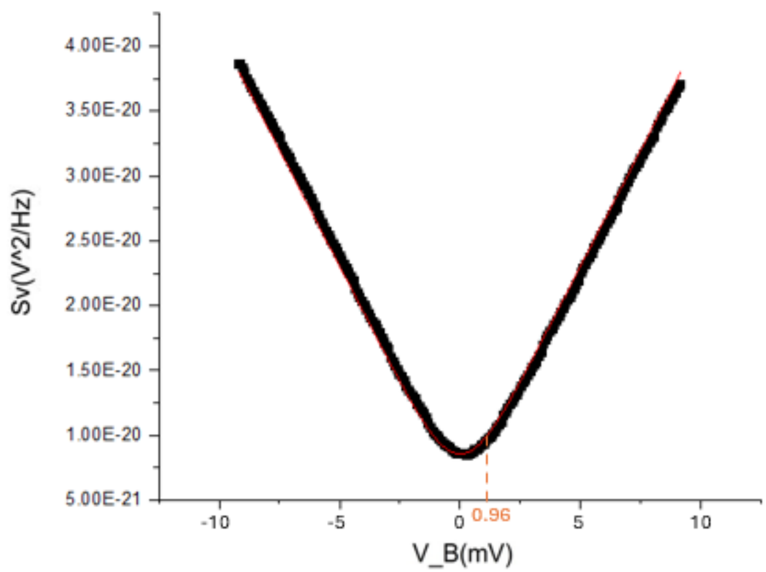

Figure 3.1: Shot noise power (S_V) versus voltage bias (V_B) data of 20nm TaN vertical junction measured at 4.3K. The red line represents the data fitting into equation (1.5). The orange number and dashed line marks the thermal broadening to linear regime crossover voltage V_{th}.

Figure 3.1 is shown to illustrate the definition of V_{th}, which helps us to better evaluate the competition between Johnson noise and shot noise. At $V_B < V_{th}$, Johnson noise tends to dominate the total noise contribution as V_B decreases. Since the voltage noise spectral density of Johnson noise is $S_{JV} = 4k_BTR$, as V_B approaches 0, the S_V vs. V_B curve becomes "flattened". We call this regime "thermal broadening" regime. As V_B increases beyond V_{th}, shot noise increases and tends to dominate the total noise contribution. The voltage noise spectral density of shot noise is $S_V = 2eV_B$, so at shot noise dominant regime, the total noise power tends to have a linear dependence on V_B, with the slope given by the Fano factor $F = \frac{S_V}{2eV_B}$. F and V_{th} are calculated in a

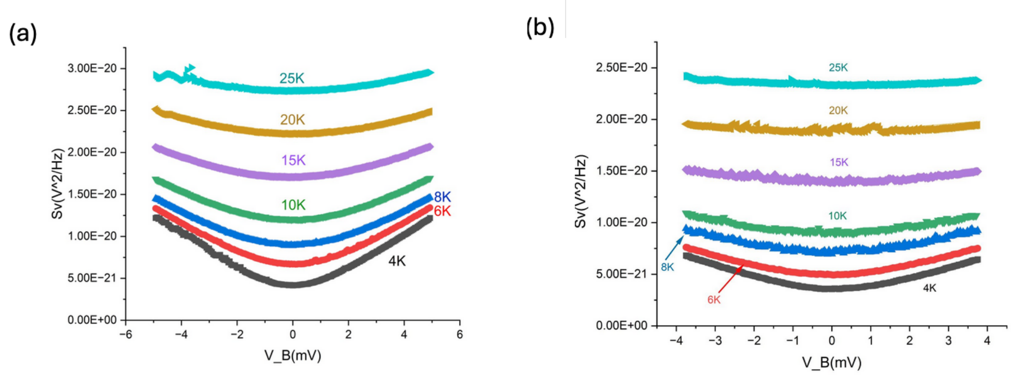

Figure 3.2: S_V vs. V_B data of 4nm βTa shown in (a) and 8nm TaN with $P_{N2} = 1 \times 10^{-4}$Torr shown in (b).

voltage bias regime large enough to cover the shot-noise-dominated regime.

The results of for 4nm βTa and 8nm TaN with partial nitrogen pressure $= 1 \times 10^{-4}$ Torr are summarized in Figure 3.2. For all samples, we fit the noise spectral density versus voltage bias data into equation (1.5) to calculate the Fano factor F and crossover voltage V_{th}. From V_{th}, we derive the thermal broadening factor $B = \frac{eV_{th}}{2k_BT}$.

We first focus on the temperature dependence of F. In Figure 3.3 (a), we observe that F decreases as T increases. As mentioned in introduction, we also found a negative temperature dependence of F in βTa nanowires with length ranging from 100nm to 2000nm[12]. Specifically, we found $F \propto 1/T$ at 100nm βTa nanowires, where $F = 0.152 \pm 0.046$ at base temperature 4.3K and decreases to $F = 0.021 \pm 0.018$ as T increases to 25K. In the introduction, we mentioned that a basic model of electron–phonon scattering described by a drift diffusion equation suggests that electron–phonon scattering is not dominant in βTa nanowires and thus not as a source of shot noise suppression. We reached this conclusion by calculating the electron-phonon coupling parameter Γ through the drift diffusion equation[23]. The 100nm and 1000nm βTa nanostrips had Γ values differed by two orders of magnitude, which should not be the case since Γ is an intrinsic property of the material. The temperature dependence of F was proposed to result from the a strong interaction between electrons. Since the Joule heat produced by the strong interaction can be poorly dissipated through either the electrode or lead, the electron temperature rises, causing electrons to flow more continuous–liquid like rather than discrete. Following this logic, at smaller length scale, the heat dissipation through lead should increase and cause an enhanced relaxation of electron heat and a approximate thermal equilibrium in the system. Under this thermal equilibrium, electron temperature should not be different from the lattice temperature, and temperature should no longer influence on the Fano factor of shot noise. However, the temperature dependence of F for 4nm, 8nm, and 20nm βTa vertical junctions was similar to 100nm to 2000nm βTa nanowires. This could suggest a flaw in our previous explanation on the electron thermal profile due to strong electron interaction. Moreover, 8nm and 20nm βTa vertical junctions show F approaching $\sqrt{3}/4$ at T=4.3K. According to the Fermi-liquid theory, $F = \sqrt{3}/4$ corresponds to the hot electron transport regime, where electrons are thermalized due to the Joule heat generated by strong electron-electron inelastic scattering. If the strong electron interaction we proposed was indeed strong electron-electron inelastic scattering and the negative temperature dependence of F is caused by this scattering mechanism, we should only see such negative dependence in the hot electron length regime(L =8nm and 20nm), not in L = 100nm and longer. The negative temperature dependence of F in βTa suggests the need for further investigation of electron thermalization mechanism in bad metal thin films.

We now focus on the results of βTa vertical junctions at the base temperature

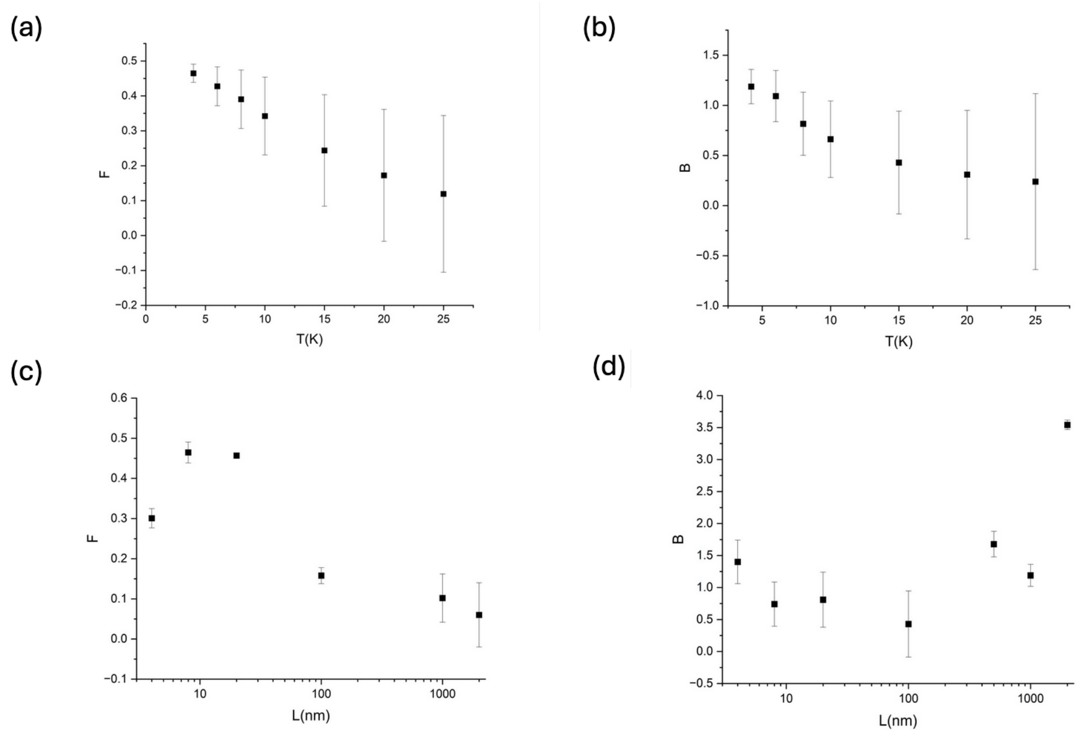

Figure 3.3: Shot noise measurement results of βTa samples. 3.3(a) and (b) show the temperature dependence of F oand B of a 8nm βTa vertical junction. 3.3(c) shows the length dependence of F measured at base temperature 4.3K. 3.3(d) shows the length dependence of B measured at base temperature 4.3K.

4.3K. Figure 3.3 (c) shows F measured from βTa samples with lengths ranging from 4nm to 2000nm. Considering the error bars, F maintains in the range of 0.425-0.475 as L decreases from 20nm to 8nm and drops to 0.29$\pm$0.052 as L further decreases to 4nm. Meanwhile, Fig.4(d) shows a weak dependence of B on L.

One major concern when comparing the Fermi-liquid, non-correlated case of F vs. L in Figure 1.1 with our experimental results is that the electron-phonon scattering mean free path can depend on temperature. Experiments on a Fermi-liquid metal have shown that $l_{e-ph} \propto 1/T^2$ at a temperature lower than 22K[24]. The theoretical prediction summarized in Figure 1.1 was experimentally confirmed at $T = 50$mK of a Fermi-liquid metal Ag[14], while our F vs. L analysis of βTa and TaN nanowires and vertical junctions are at base temperature 4.3K. Therefore, if we want to compare our results of βTa and TaN with the Fermi-liquid values, Figure 1.1 should be rewritten as Figure 3.4 to control the temperature parameter.

The length dependence of F of βTa looks similar to the Fermi-liquid prediction. In our previous study on βTa nanostrips, we found F decreases by a modest amount compared to uncertainty as L increases and approximately scaled as $1/L$. The largest F was 0.16$\pm$0.02 at shortest length L = 100nm.

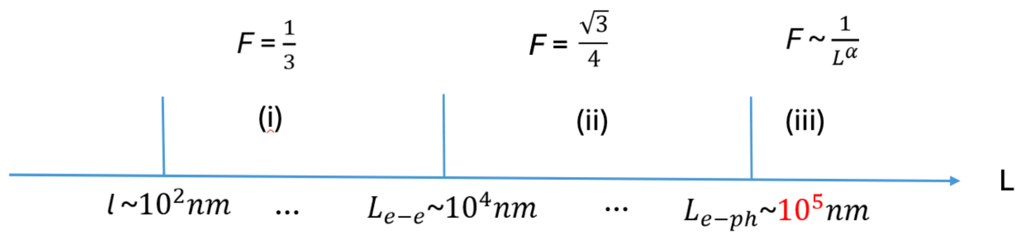

Figure 3.4: Fermi liquid prediction of electron scattering length and F vs. L taking into account the temperature dependence of L_{e-ph}

If we only look at the values of F, then 100nm$< L <$ 2000nm of βTa behaves the same as in regime (iii) of Figure 3.4, which is the electron-phonon scattering dominant regime with $\alpha = 1$. As L of βTa decreases to 20nm and 8nm, F becomes close to $\frac{\sqrt{3}}{4} = 0.4330127...$ which seems to fall in regime(ii), the strong electron-electron scattering regime. At $L = 4$nm, F drops to 0.30 ± 0.025, which is close to 1/3 as in regime (i).

However, although the trend of F with respect to L of βTa seems to look like following the Fermi-liquid, non-correlated prediction, they are actually different in the following two ways.

First, as we mentioned, electron-phonon scattering was ruled out as a source of the suppression of F for βTa nanowires with 100nm$< L <$ 2000nm. Therefore, although the behavior of F seems consistent, shot noise suppression of βTa at 100nm$< L <$

2000nm cannot be explained by electron-phonon scattering as in Fermi liquid theory.

Second, the strong electron-electron inelastic scattering mean free paths of βTa is much shorter than the Fermi-liquid system. As shown in Figure 1.1, L_{e-e} of a Fermi-liquid system is around 1×10^4nm. However, F of βTa increases from around 1/3 to $\frac{\sqrt{3}}{4}$ as L jumps from 4nm to 8nm, meaning that the electron-electron inelastic scattering mean free path L_{e-e} of βTa should be in between 4nm and 8nm–three orders of magnitude smaller than the Fermi-liquid system. In bad metal βTa, an electron travel a three times smaller length than in Fermi liquid to scatter with another electron inelastically and generate Joule heat to the system. The high probability of electron-electron inelastic scattering can impedes the electron flow in the material, resulting in a high resistivity approaching the Ioffe-Regel limit. On the other hand, this small value of L_{e-e} can hold under Fermi-liquid picture. As mentioned in Chapter 1, a recent study has proposed that $F = \frac{\sqrt{3}}{4}$ indicates a strong correlation of electrons[9]. In this study, the Boltzman-Langevin equation was derived in the presence of quasi-particles with a strong correlation term introduced. The strong electron interaction in βTa can contribute to a strong correlation of electrons which results in $F = \frac{\sqrt{3}}{4}$ while the quasiparticles maintain well-defined.

We now discuss our shot noise measurement results of TaN vertical junctions. Figure 3.5 summarizes the results of TaN vertical junctions with a partial nitrogen pressure $P_{N2} = 1 \times 10^{-4}$Torr. Figure 3.5(a) shows that, given the relatively large error bar, F exhibits a decreasing trend as T increases. On the other hand, Figure 3.5(b) shows that B has a weak dependence on T. The temperature dependence of F and B of TaN is consistent to βTa.

Figure 3.5(c) shows that as L increases from 4nm to 20nm, F of TaN maintains close to $\frac{1}{3}$, considering the error bar. This value matches with the diffusive transport regime in the Fermi-liquid picture(regime(i) in Figure 3.4). We compare Figure 3.5(c) with Figure 3.3(c). At 4nm, βTa and TaN both have $\frac{1}{3}$ Fano factor. However, at

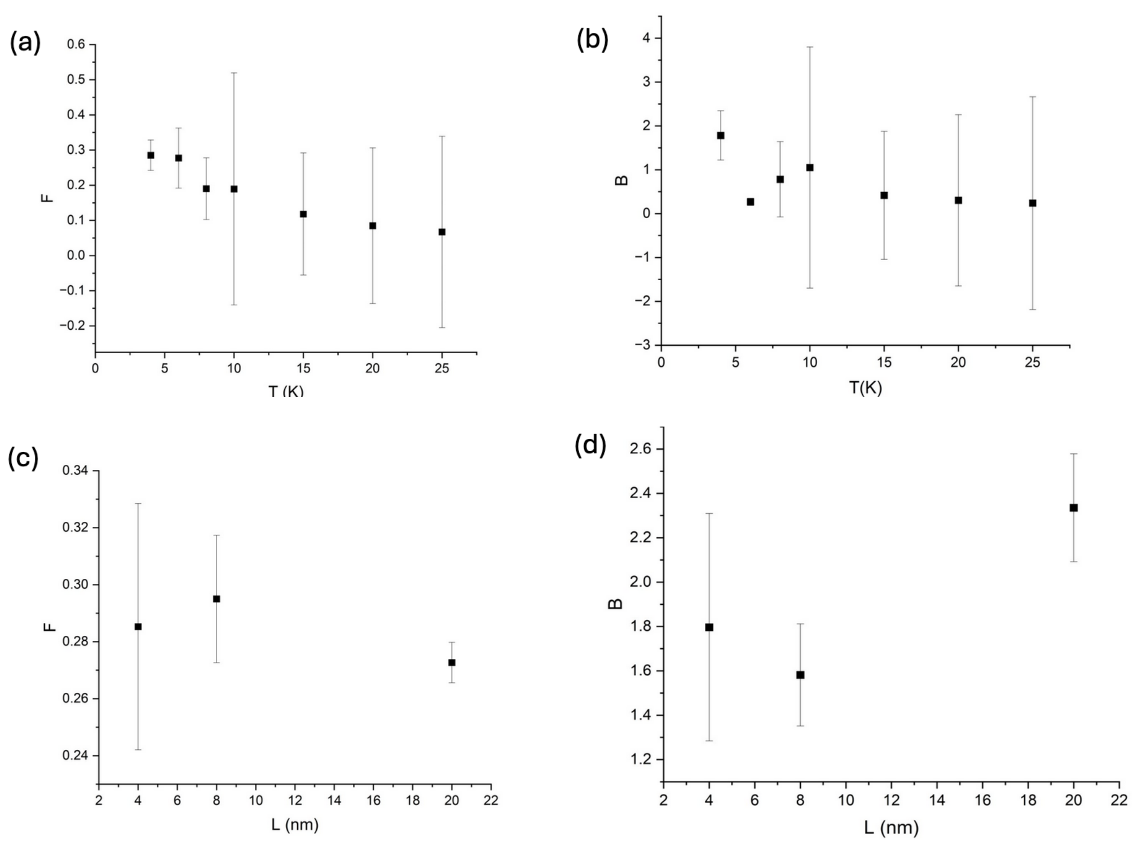

Figure 3.5: Shot noise measurement results of TaN vertical junctions at $P_{N2} = 1 \times 10^{-4}$ Torr. 3.3(a) and (b) show the temperature dependence of F and B of a 4nm TaN vertical junction. 3.3 (c) and (d) shows the length dependence of F and B measured at base temperature 4.3K.

8nm, βTa enters the hot electron transport regime where $F = \frac{\sqrt{3}}{4}$, while TaN stays in diffusive transport regime. One possibility can be that L_{e-e} of TaN is longer than βTa. This contradicts with the explanation of the disorder of TaN lattice. As mentioned in Chapter 1, previous studies have shown an increased nitrogen pressure during Ta development can lead to an increase of lattice disorder. As the lattice structure becomes more disordered, electrons experience more frequent inelastic scattering with more randomly positioned lattice sites or irregular lattice defects. Therefore, l_{e-e} is smaller in TaN than βTa. As disorder increases even more, the electrons can be localized due to constructive interference of their multiple scattered wavefunctions — a phenomenon known as Anderson localization[25]. When this happens, electrons are no longer able to transport diffusively through the material. Instead, their wavefunctions decay exponentially with the distance from their localized position, resulting in a highly localized state of electron in real space. As the disorder increases to some some critical disorder strength, the material's behavior turns from a metal to an insulator[26]. This logic can explain the metal-to insulator transition of TaN: as P_{N2} increases, the disorder in the TaN lattice also increases and causes to a strong electron localization when P_{N2} approaches 6×10^{-4}Torr. However, Figure (c) suggests the opposite trend: L_{e-e} of TaN is larger than βTa. The explanation for this requires further investigation. In the future, we will reproduce the TaN vertical junctions samples to verify this argument.

Figure 3.5(d) shows that the thermal broadening factor B of TaN does not have a significant dependence on L. The values are larger than 1 which corresponds to the diffusive transport regime of Fermi liquid.

We finally discuss our Hall measurement results of TaN. We apply a constant DC current $I = 100$mA to the horizontal hall bar and measured the Hall voltage V_H at vertical direction as the perpendicular magnetic field B is tuned. Differential resistance $R = \frac{dV_H}{dI}$ was calculated and plotted as a function of B.

From this set up, we want to derive the charge carrier density n. The Coulomb force of charges balances with the Lorenz force, giving

$$\vec{E} = \vec{v} \times \vec{B}. \tag{3.1}$$

We simplify the model as such: the electric field points at the vertical(y) direction and the current flows in the horizontal(x) direction. (3.1) thus becomes

$$E_y = v_x B. \tag{3.2}$$

The current density is defined as

$$j_x = nqv_x, \tag{3.3}$$

where n is the number density of charge carriers, q is the unit charge. Thus,

$$E_y = \frac{j_x B}{ne}. \tag{3.4}$$

On the other hand, the definition of electric field gives

$$E_y = \frac{V_H}{w_2}, \tag{3.5}$$

where V_H is the Hall voltage and $w_2 = 3\mu$m is the vertical effective length of the Hall cross shown in Figure 2.5. Combining equation (3.4) and (3.5) gives

$$V_H = \frac{j_x B w_2}{ne}. \tag{3.6}$$

The current density is also expressed as

$$j_x = \frac{I_x}{A}, \tag{3.7}$$

where I_x is the current applied to the horizontal electrode and A is the cross-sectional area of the horizontal Hall bar. Also,

$$A = w_1 t, \tag{3.8}$$

where $L_2 = 3.26\mu$m is the width of the horizontal Hall bar and $t = 20$nm is the thickness of the horizontal Hall bar. Plugging equation(3.7) and (3.8) into (3.6), we arrive at

$$V_H = \frac{I_x}{w_1 t}\frac{Bw_2}{ne}. \tag{3.9}$$

Therefore we have

$$n = \frac{B}{(\frac{V_H}{I_x})}\frac{w_2}{w_1}\frac{1}{t}, \tag{3.10}$$

where $\frac{B}{(\frac{V_H}{I_x})}$ is the inverse of the slope of the differential resistance verses magnetic field data that we measured.

At 20K, the slope for $P_{N_2} = 1 \times 10^{-4}$Torr was $1.19 \times 10^{-8}\Omega$/Oe, which is $1.19 \times 10^{-4}\Omega$/T, and the charge carrier density was calculated as $n_{low} = 3.94 \times 10^{24} cm^{-3}$. The slope for $P_{N_2} = 4 \times 10^{-4}$ is $8.95 \times 10^{-4}\Omega$/T, and $n_{high} = 4.63 \times 10^{23} cm^{-3}$. The result contradicts to our hypothesis. As partial nitrogen pressure increases, if the crystal lattice of TaN becomes more disordered, the charge carrier should concentrate more in the conductor and the charge density should increase. The order of magnitude of n of TaN is more than one order of magnitude larger than the typical value of $10^{22} cm^{-3}$, making the values not trustable. The unexpected low order of magnitude of the charge carrier density can be due to that when $Im(7)$ was performed to remove the $Au(5)$ layer, the actual ion-milling depth was less than 7nm because of poor calibration. From previous Hall measurement on TaN in our group, we knew that charge transport in TaN is hole-like, while charge transport in Au is electron-like. When current is applied under the magnetic field, the charge carriers will move the opposite ways in TaN and Au layers due to the different sign of the Lorentz force. The Hall voltage in TaN layer and Au layer will therefore have different sign. Since the total Hall voltage of the Hall bar sample equals to the summation of Hall voltage in Au and TaN layer(the two layers can be considered as parallel in the circuit), it will be smaller than the Hall bar with only TaN layer where Au is completely milled off. From equation(3.10), a smaller V_H will give us larger n. This error is confirmed by the sheet resistance of our TaN hall bar with an aspect ratio 1/3, which is 200Ω at room temperature. However, at room temperature, the resistivity of TaN with $P_{N2} = 1 \times 10^{-4}$is around $3500 n\Omega$m, and the sheet resistance is around 1166Ω. The lower-than-expected resistance of our TaN sample can be contributed to the Au residue layer on the top due to insufficient ion-milling. In our future experiment, we will calibrate the the ion-milling rate to ensure the Au layer on top of TaN layer is completely milled-off.

Chapter 4

Conclusion

In this experiment, we fabricated βTa and TaN vertical junctions and conducted shot noise measurement. We calculated shot noise Fano factor and thermal broadening factor and plotted them as functions of temperature and length. For βTa vertical junctions, we found $\frac{1}{3}$ Fano factor at 4nm and $\frac{\sqrt{3}}{4}$ Fano factor at 8nm and 20nm. From the values of Fano factor, we observed that the length scale of strong electron-electron inelastic scattering mean free path is much smaller than the Fermi-liquid material. The frequent electron-electron inelastic scattering in βTa can impedes the flow of electrons in the material and contribute to the high resistivity of βTa. A strong correlation of electrons can also be inferred in the hot electron scattering regime of βTa. The anomalous temperature dependence of shot noise also opens windows to further explore electron thermalization mechanism of bad metals. Further shot noise measurements at lower temperature that our cryostat cannot approach can provide more insights the thermalization mechanism of inelastic electron scattering. The source of suppression of βTa nanowires with lengths ranging from 100nm to 2000nm is still unclear and deviates from the Fermi liquid theory. A more thorough model of electron-phonon scattering in metallic thin film can be developed to describe βTa nanowires considering multiple ways of thermal relaxation(through electrodes and substrates). Further investigation on lattice disorder in βTa can also provide insights of the source of the suppression of shot noise and lead to further knowledge of disorder effects on non-Fermi liquid systems.

For TaN, we found 1/3 Fano factor at 4nm, 8nm, and 20nm and B all close to 1. Based on the disorder statement of Ta, we argue that the electron-electron inelastic scattering mean free path in TaN should decreased by the disorder of lattice of tantalum tuned by nitrogen pressure. The opposite trend of F values in TaN will be verified by further shot noise measurement in TaN vertical junctions. The disorder of a system can be evaluated through charge carrier density. In our experiment, we explored the sample design and measurement setup for Hall measurement of TaN and gained experience for further Hall measurements. With such experience, we will continue to perform Hall measurements on TaN Hall bars grown under different nitrogen partial pressures and with different lengths and explore the shot noise behaviors.

Bibliography

[1] H. J. Schulz. Fermi liquids and non–fermi liquids, 1995.

[2] R. W. Hill, Cyril Proust, Louis Taillefer, P. Fournier, and R. L. Greene. Breakdown of fermi-liquid theory in a copper-oxide superconductor. *Nature*, 414(6865):711–715, December 2001.

[3] Philip Phillips, Ting-Pong Choy, and Robert G. Leigh. Breakdown of fermi liquid theory in doped mott insulators by dynamical spectral weight transfer, 2008.

[4] Liyang Chen, Dale T. Lowder, Emine Bakali, Aaron Maxwell Andrews, Werner Schrenk, Monika Waas, Robert Svagera, Gaku Eguchi, Lukas Prochaska, Yiming Wang, Chandan Setty, Shouvik Sur, Qimiao Si, Silke Paschen, and Douglas Natelson. Shot noise in a strange metal. *Science*, 382(6673):907–911, 2023.

[5] Debanjan Chowdhury, Antoine Georges, Olivier Parcollet, and Subir Sachdev. Sachdev-ye-kitaev models and beyond: Window into non-fermi liquids. *Rev. Mod. Phys.*, 94:035004, Sep 2022.

[6] Qikai Guo, César Magén, Marcelo J. Rozenberg, and Beatriz Noheda. Phenomenological classification of metals based on resistivity. *Phys. Rev. B*, 106:085141, Aug 2022.

[7] Netanel H. Lindner and Assa Auerbach. Conductivity of hard core bosons: A paradigm of a bad metal. *Phys. Rev. B*, 81:054512, Feb 2010.

[8] V. J. Emery and S. A. Kivelson. Superconductivity in bad metals. *Phys. Rev. Lett.*, 74:3253–3256, Apr 1995.

[9] Yiming Wang, Chandan Setty, Shouvik Sur, Liyang Chen, Silke Paschen, Douglas Natelson, and Qimiao Si. Shot noise and universal fano factor as a characterization of strongly correlated metals. *Phys. Rev. Res.*, 6:L042045, Nov 2024.

[10] M. J. M. de Jong and C. W. J. Beenakker. Shot noise in mesoscopic systems, 1996.

[11] Yiou Zhang, Shashi Pandey, Sergei Ivanov, Jian Liu, and Sergei Urazhdin. Shot noise in a metal close to the mott transition. *Nano Letters*, 24(50):15943–15949, 2024. PMID: 39653590.

[12] Mateusz Szurek, Hanqiao Cheng, Zilu Pang, Yiou Zhang, John Bacsa, and Sergei Urazhdin. Anomalous shot noise in a bad metal -tantalum. *Applied Physics Letters*, 126(8):082410, 02 2025.

[13] Ya.M. Blanter and M. Büttiker. Shot noise in mesoscopic conductors. *Physics Reports*, 336(1–2):1–166, September 2000.

[14] Andrew H. Steinbach, John M. Martinis, and Michel H. Devoret. Observation of hot-electron shot noise in a metallic resistor. *Phys. Rev. Lett.*, 76:3806–3809, May 1996.

[15] C. W. J. Beenakker and M. Büttiker. Suppression of shot noise in metallic diffusive conductors. *Phys. Rev. B*, 46:1889–1892, Jul 1992.

[16] K. E. Nagaev. Influence of electron-electron scattering on shot noise in diffusive contacts. *Phys. Rev. B*, 52:4740–4743, Aug 1995.

[17] K. Lal, P. Ghosh, D. Biswas, A.K. Meikap, S.K. Chattopadhyay, S.K. Chatterjee, M. Ghosh, K. Baba, and R. Hatada. A low temperature study of electron

transport properties of tantalum nitride thin films prepared by ion beam assisted deposition. *Solid State Communications*, 131(7):479–484, 2004.

[18] Natalia Kovaleva, Dagmar Chvostova, and Alexandr Dejneka. Localization phenomena in disordered tantalum films. *Metals*, 7(7):257, July 2017.

[19] Saumyadip Chaudhuri, Ilari J. Maasilta, Lucie Chandernagor, Marion Ging, and Manu Lahtinen. Fabrication of superconducting tantalum nitride thin films using infrared pulsed laser deposition. *Journal of Vacuum Science Technology A*, 31(6):061502, 07 2013.

[20] Nicholas P. Breznay, Mihir Tendulkar, Li Zhang, Sang-Chul Lee, and Aharon Kapitulnik. Superconductor to weak-insulator transitions in disordered tantalum nitride films. *Phys. Rev. B*, 96:134522, Oct 2017.

[21] Masatoshi Imada, Atsushi Fujimori, and Yoshinori Tokura. Metal-insulator transitions. *Rev. Mod. Phys.*, 70:1039–1263, Oct 1998.

[22] Niravkumar D. Patel, Anamitra Mukherjee, Nitin Kaushal, Adriana Moreo, and Elbio Dagotto. Non-fermi liquid behavior and continuously tunable resistivity exponents in the anderson-hubbard model at finite temperature. *Phys. Rev. Lett.*, 119:086601, Aug 2017.

[23] M. Henny, H. Birk, R. Huber, C. Strunk, A. Bachtold, M. Krüger, and C. Schönenberger. Electron heating effects in diffusive metal wires. *Applied Physics Letters*, 71(6):773–775, 08 1997.

[24] R. N. Jana, S. Sinha, and A. K. Meikap. Linear mean free path and quadratic temperature dependence of electron-phonon scattering rate in v82al18-xfex alloys at low temperature. *AIP Advances*, 5(5):057110, 05 2015.

[25] Chen Guan and Xingyue Guan. A brief introduction to anderson localization. 2019.

[26] Krzysztof Byczuk, Walter Hofstetter, and Dieter Vollhardt. Anderson localization vs. mott–hubbard metal–insulator transition in disordered, interacting lattice fermion systems. *International Journal of Modern Physics B*, 24(12n13):1727–1755, May 2010.